frontiers in Cell and Developmental Biology

ORIGINAL RESEARCH
published: 28 July 2020
doi: 10.3389/fcell.2020.00536

Ultrarapid Delayed Rectifier K^+ Channelopathies in Human Induced Pluripotent Stem Cell-Derived Cardiomyocytes

Sarah Hilderink[1], Harsha D. Devalla[1], Leontien Bosch[1], Ronald Wilders[1] and Arie O. Verkerk[1,2]*

[1] Department of Medical Biology, Amsterdam UMC, University of Amsterdam, Amsterdam, Netherlands, [2] Department of Experimental Cardiology, Amsterdam UMC, University of Amsterdam, Amsterdam, Netherlands

Atrial fibrillation (AF) is the most common cardiac arrhythmia. About 5–15% of AF patients have a mutation in a cardiac gene, including mutations in *KCNA5*, encoding the $K_v1.5$ α-subunit of the ion channel carrying the atrial-specific ultrarapid delayed rectifier K^+ current (I_{Kur}). Both loss-of-function and gain-of-function AF-related mutations in *KCNA5* are known, but their effects on action potentials (APs) of human cardiomyocytes have been poorly studied. Here, we assessed the effects of wild-type and mutant I_{Kur} on APs of human induced pluripotent stem cell-derived cardiomyocytes (hiPSC-CMs). We found that atrial-like hiPSC-CMs, generated by a retinoic acid-based differentiation protocol, have APs with faster repolarization compared to ventricular-like hiPSC-CMs, resulting in shorter APs with a lower AP plateau. Native I_{Kur}, measured as current sensitive to 50 μM 4-aminopyridine, was 1.88 ± 0.49 (mean ± SEM, n = 17) and 0.26 ± 0.26 pA/pF (n = 17) in atrial- and ventricular-like hiPSC-CMs, respectively. In both atrial- and ventricular-like hiPSC-CMs, I_{Kur} blockade had minimal effects on AP parameters. Next, we used dynamic clamp to inject various amounts of a virtual I_{Kur}, with characteristics as in freshly isolated human atrial myocytes, into 11 atrial-like and 10 ventricular-like hiPSC-CMs, in which native I_{Kur} was blocked. Injection of I_{Kur} with 100% density shortened the APs, with its effect being strongest on the AP duration at 20% repolarization (APD_{20}) of atrial-like hiPSC-CMs. At I_{Kur} densities < 100% (compared to 100%), simulating loss-of-function mutations, significant AP prolongation and raise of plateau were observed. At I_{Kur} densities > 100%, simulating gain-of-function mutations, APD_{20} was decreased in both atrial- and ventricular-like hiPSC-CMs, but only upon a strong increase in I_{Kur}. In ventricular-like hiPSC-CMs, lowering of the plateau resulted in AP shortening. We conclude that a decrease in I_{Kur}, mimicking loss-of-function mutations, has a stronger effect on the AP of hiPSC-CMs than an increase, mimicking gain-of-function mutations, whereas in ventricular-like hiPSC-CMs such increase results in AP shortening, causing their AP morphology to become more atrial-like. Effects of native I_{Kur} modulation on atrial-like hiPSC-CMs are less pronounced than effects of virtual I_{Kur} injection because I_{Kur} density of atrial-like hiPSC-CMs is substantially smaller than that of freshly isolated human atrial myocytes.

Keywords: atrial fibrillation, cardiac differentiation, dynamic clamp, human pluripotent stem cells, ion channels, *KCNA5*, $K_v1.5$, ultrarapid delayed rectifier potassium current

OPEN ACCESS

Edited by:
Jong-Kook Lee,
Osaka University, Japan

Reviewed by:
Haibo Ni,
University of California, Davis, United States
Andrea Barbuti,
University of Milan, Italy

****Correspondence:***
Ronald Wilders
r.wilders@amsterdamumc.nl

Specialty section:
This article was submitted to Stem Cell Research, a section of the journal Frontiers in Cell and Developmental Biology

Received: *31 March 2020*
Accepted: *08 June 2020*
Published: *28 July 2020*

Citation:
Hilderink S, Devalla HD, Bosch L, Wilders R and Verkerk AO (2020) Ultrarapid Delayed Rectifier K^+ Channelopathies in Human Induced Pluripotent Stem Cell-Derived Cardiomyocytes. Front. Cell Dev. Biol. 8:536. doi: 10.3389/fcell.2020.00536

INTRODUCTION

Worldwide, the prevalence of atrial fibrillation (AF) is around 1–2% (Potpara and Lip, 2011). Mutations in cardiac genes account for onset of 5–15% of AF cases (Darbar et al., 2003; Potpara and Lip, 2011). Mutations in *KCNA5* are associated with AF, although rare (Feghaly et al., 2018). *KCNA5* encodes the pore-forming α-subunit $K_v1.5$ of the channel carrying the ultrarapid delayed rectifier K^+ current (I_{Kur}) (Fedida et al., 1993; Wang et al., 1993). In the human heart, $K_v1.5$ and the mRNA encoding $K_v1.5$ are both highly expressed in the atria (Ellinghaus et al., 2005; Gaborit et al., 2007), whereas expression of $K_v1.5$ is very low in both endocardial and epicardial ventricular tissue (Mays et al., 1995; Gaborit et al., 2007) and expression of mRNA encoding $K_v1.5$ is also low (Kääb et al., 1998; Gaborit et al., 2007). Accordingly, in their voltage clamp experiments on isolated human atrial and subepicardial ventricular myocytes, Amos et al. (1996) could not observe an I_{Kur}-like current in their ventricular myocytes, in contrast to their atrial myocytes. I_{Kur} activates rapidly upon depolarizations to membrane potentials positive to −50 mV and is responsible for the early repolarization in human atrial action potentials (APs) (Wang et al., 1993; Amos et al., 1996; Wettwer et al., 2004; Li et al., 2008).

Both loss-of-function and gain-of-function mutations in *KCNA5* have been identified in patients with AF (Olson et al., 2006; Yang et al., 2009, 2010; Christophersen et al., 2013; Hayashi et al., 2015; Tian et al., 2015). Loss-of-function mutations in *KCNA5* are supposed to increase susceptibility to AF by prolonging the AP duration (APD) of atrial myocytes, which may eventually result in early afterdepolarizations (EADs) (Yang et al., 2009; Hayashi et al., 2015). Indeed, *in vitro* electrophysiological studies where I_{Kur} was blocked, representing complete *KCNA5* loss-of-function mutations, resulted in prolonged APDs and presence of EADs (Olson et al., 2006). EADs as a consequence of prolonged APDs have also been observed in *in silico* studies on loss-of-function *KCNA5* mutations (Colman et al., 2017; Ni et al., 2017).

Gain-of-function mutations, on the other hand, are presumed to cause AF by shortening the effective refractory period (ERP) of the atrial AP, facilitating re-entry wavelets in the atria (Nattel, 2002; Christophersen et al., 2013). This hypothesis is supported by *in silico* studies, which demonstrated that increased I_{Kur} density, representing gain-of-function mutations, resulted in a shortened APD and arrhythmogenesis in human atrial tissue (Colman et al., 2017; Ni et al., 2017).

Although the *in silico* studies are instrumental in determining the potential effect of both loss-of-function and gain-of-function mutations in *KCNA5*, detailed electrophysiological studies of the *KCNA5* mutations in human cardiomyocytes are limited. Human induced pluripotent stem cell cardiomyocytes (hiPSC-CMs) have become a highly suitable tool to study cardiac ion channelopathies and their electrophysiology (Zhang et al., 2011; Hoekstra et al., 2012; Verkerk et al., 2017). Over time, the technique of cardiomyocyte differentiation has advanced, facilitating the generation of distinct atrial- and ventricular-like hiPSC-CM populations (Zhang et al., 2011; Devalla et al., 2015; Devalla and Passier, 2018). In the present study, we employed dynamic clamp to investigate the effects of loss-of-function and gain-of-function mutations in *KCNA5* in both atrial- and ventricular-like hiPSC-CMs.

MATERIALS AND METHODS

hiPSC-CM Differentiation

hiPSC-CMs were generated from the control LUMC0099iCTRL04 hiPSC line, which was derived from human fibroblasts extracted through skin biopsies from of a Caucasian woman. The LUMC0099iCTRL04 line is registered in the Human Pluripotent Stem Cell Registry (Seltmann et al., 2016), which contains all details pertaining to its generation and characterization (hPSCreg, 2019). hiPSC clones showing stem cell morphology were characterized for pluripotency marker expression and differentiation potential to hiPSC-CMs in BPEL medium (Ng et al., 2008) containing activin-A, BMP4, and CHIR99021 (Devalla et al., 2016). After 3 days, this medium was replaced by BPEL medium containing XAV939 (Tocris Biosciences) for ventricular differentiation (Ng et al., 2008; Devalla et al., 2016). To differentiate hiPSC-CMs to atrial-like hiPSC-CMs, 1 μM all-trans retinoic acid (RA) was added (Devalla et al., 2015). Twenty days after differentiation, hiPSC-CMs were dissociated with TrypLE Select (Life Technologies), and plated at a low density (≈7.5×10^4 cells) on Matrigel coated coverslips in BPEL medium (Devalla et al., 2016).

Patch-Clamp Measurements

Data Acquisition

Electrophysiological recordings were performed 4–13 days post dissociation from spontaneously beating single hiPSC-CMs. RA-treated hiPSC-CMs displaying a short, pulse-like beating pattern and non-RA-treated hiPSC-CMs with a contraction-like beating pattern were selected for data acquisition. APs and I_{Kur} were recorded at 36–37°C with the perforated patch-clamp technique using an Axopatch 200B amplifier (Molecular Devices, Sunnyvale, CA, United States). Data acquisition and analysis were performed with custom software. Signals were low-pass filtered with a cut-off frequency of 2 kHz and digitized at 40 and 5 kHz for AP and I_{Kur} recordings, respectively. Cell membrane capacitance (C_m, in pF) was calculated by dividing the time constant of the decay of capacitive transient when hyperpolarized by 5 mV from −40 mV in voltage clamp by series resistance. C_m of atrial- and ventricular-like hiPSC-CMs was 16.4 ± 2.3 pF (mean ± SEM, n = 28), and 19.2 ± 2.5 pF (n = 27), respectively (t-test, N.S.). Patch pipettes with a resistance of ≈2.0 MΩ were pulled from borosilicate glass (Harvard Apparatus) and filled with solution containing (in mM): 125 K-gluconate, 20 KCl, 5 NaCl, 0.44 Amphotericin-B, 10 HEPES; pH set to 7.2 (KOH). Cells were superfused with modified Tyrode's solution containing (in mM): 140 NaCl, 5.4 KCl, 1.8 $CaCl_2$, 1.0 $MgCl_2$, 5.5 D-glucose, 5 HEPES; pH set to 7.4 (NaOH). All potentials were corrected for the estimated liquid junction potential of −15 mV (Barry and Lynch, 1991).

Action Potential Recordings

APs were elicited at 1 Hz by 3-ms, ≈1.2 × threshold current pulses through the patch pipette. The AP parameters analyzed were resting membrane potential (RMP, in mV), maximum upstroke velocity (dV/dt_{max}, in V/s), AP amplitude (APA, in mV), AP duration at 20, 50, and 90% repolarization (APD_{20}, APD_{50}, and APD_{90}, respectively, in ms), and AP plateau amplitude (APPlatA, in mV), derived from the membrane potential (V_m) at 50 ms after the time of dV/dt_{max}.

Native I_{Kur} Recordings

Native I_{Kur} was activated by 200-ms voltage clamp steps from −50 to +50 mV. A 50-ms prepulse to 0 mV was applied to activate and inactivate remaining transient membrane currents. Series resistance was compensated by ≥ 80%. I_{Kur} was measured as the current sensitive to 50 μM 4-aminopyridine (4-AP) (Wang et al., 1993; Caballero et al., 2010), and was normalized to C_m to calculate current density (in pA/pF).

Dynamic Clamp

Although inward rectifier K^+ current (I_{K1}) is not necessarily low in hiPSC-CMs (Horváth et al., 2018), hiPSC-CMs tend to lack I_{K1}, which is responsible for stabilizing the RMP of atrial and ventricular myocytes, and thus show spontaneous activity (Dhamoon and Jalife, 2005; Hoekstra et al., 2012; Verkerk et al., 2017). The RMP of our atrial- and ventricular-like hiPSC-CMs was stabilized and set at a regular hyperpolarized value using the dynamic clamp technique (Wilders, 2006). A virtual Kir2.1-based I_{K1}, with a standard peak current density of 2 pA/pF, was injected into the hiPSC-CMs and this I_{K1} was computed in real time, based on the acquired V_m, following the approach of Meijer van Putten et al. (2015). Accordingly, the mathematical equation for I_{K1} reads

$$I_{K1} = 0.12979 \times \left(\frac{V_m - E_K}{1.0 + e^{(0.093633 \times (V_m + 72))}} \right)$$

In this equation, in which the rectification properties of I_{K1} are implemented through a Boltzmann equation, I_{K1} is in pA/pF and V_m is in mV. E_K is the Nernst potential for potassium, which amounts to −86.9 mV in our experimental setting.

The effect of the injection of this virtual I_{K1} is illustrated in **Figure 1**, which shows the APs of typical atrial-like and ventricular-like hiPSC-CMs in the absence and presence of this virtual I_{K1} (top panels) and the associated injected current (bottom panels), which consists of this I_{K1} and a short inward stimulus current. A virtual Kir2.1-based I_{K1}, characteristic for human ventricular myocytes (Wang et al., 1998), was used in both atrial- and ventricular-like hiPSC-CMs because a more 'atrial-like' I_{K1} in hiPSC-CMs results in a substantial current during early repolarization due to its reduced rectification (Meijer van Putten et al., 2015; Verkerk et al., 2017; Fabbri et al., 2019), and we wanted to prevent a prominent overlap and potential interference of I_{K1} and I_{Kur} during the course of an action potential.

The dynamic clamp technique was also used to provide our atrial- and ventricular-like hiPSC-CMs with a virtual wild-type or mutant I_{Kur}, as illustrated in **Figure 2**. Like I_{K1}, I_{Kur} was computed in real time, based on the acquired value of V_m. I_{Kur} was formulated as detailed in Section "I_{Kur} Equations" below. Virtual I_{Kur} was injected into atrial- and ventricular-like hiPSC-CMs with a fully activated conductance of 12.5, 25, 50, and 75% of its wild-type value to mimic loss-of-function mutations, and 125, 150, 175, and 200% of its wild-type value to mimic gain-of-function mutations.

I_{Kur} Equations

To compute I_{Kur} in our dynamic clamp system, I_{Kur} equations of the comprehensive human atrial myocyte model by Maleckar et al. (2009) were used. These equations were also adopted by Grandi et al. (2011) in their human atrial action potential and Ca^{2+} model and read:

$$I_{Kur} = g_{Kur} \times a_{ur} \times i_{ur} \times (V - E_K)$$

$$da_{ur}/dt = (a_{ur,\infty} - a_{ur}) / \tau_{aur}$$

$$di_{ur}/dt = (i_{ur,\infty} - i_{ur}) / \tau_{iur}$$

$$a_{ur,\infty} = \frac{1.0}{\left[1.0 + e^{-(V + \frac{6.0}{8.6})}\right]}$$

$$i_{ur,\infty} = \frac{1.0}{\left[1.0 + e^{(V + \frac{7.5}{10.0})}\right]}$$

$$\tau_{aur} = \frac{0.009}{\left[1.0 + e^{(V + \frac{5.0}{12.0})}\right]} + 0.0005$$

$$\tau_{iur} = \frac{0.59}{\left[1.0 + e^{(V + \frac{60.0}{10.0})}\right]} + 3.05$$

In these equations, the dimensionless Hodgkin and Huxley-type activation and inactivation gating variables, ranging between 0 and 1, are denoted by a_{ur} and i_{ur}, respectively, whereas I_{Kur} (in pA/pF), g_{Kur} (in nS/pF), V (in mV), E_K (in mV), and t (in s) denote the ultrarapid delayed rectifier outward K^+ current, its fully activated conductance, the membrane potential, the K^+ reversal potential, and the time, respectively. The steady-state values of a_{ur} and i_{ur} are denoted by $a_{ur,\infty}$ and $i_{ur,\infty}$, respectively, and the associated time constants by τ_{aur} (in s) and τ_{iur} (in s), respectively. As in the models by Maleckar et al. (2009) and Grandi et al. (2011), a default value of 0.045 nS/pF was used for g_{Kur}. Of note, Maleckar et al. (2009) based this value on experimental data on I_{Kur} density in human atrial myocytes.

Statistical Analysis

Data are presented as mean ± SEM. Statistical analysis was carried out with SigmaStat 3.5 software (Systat Software, Inc., San Jose, CA, United States). Native I_{Kur} density of atrial- and ventricular-like hiPSC-CMs was compared with an independent samples *t*-test. Two-way repeated measures ANOVA followed by the Student–Newman–Keuls *post hoc* test was used for

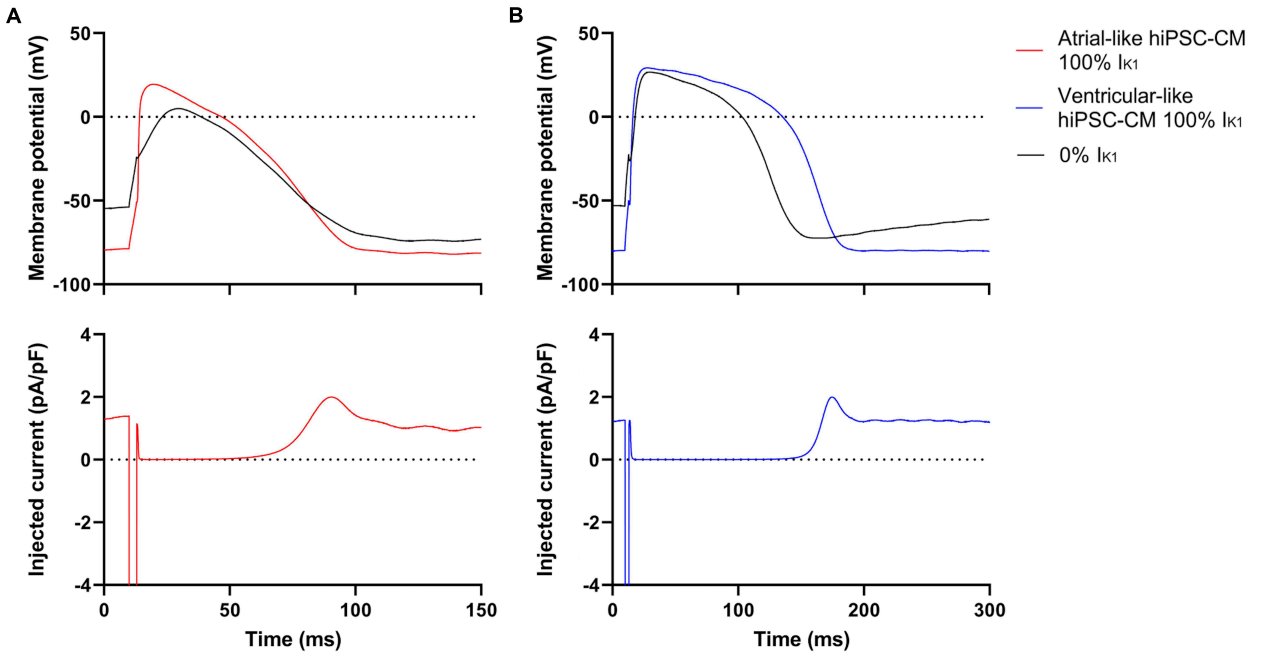

FIGURE 1 | Typical action potentials (APs) of atrial- and ventricular-like hiPSC-CM with and without I_{K1} injection. **(A)** Superimposed APs (top panel) of an atrial-like hiPSC-CM in absence (black line) and presence (red line) of 100% virtual I_{K1} injected through dynamic clamp and associated injected current (bottom panel) consisting of stimulus current and 0% or 100% virtual I_{K1}. **(B)** Superimposed APs and associated injected current of a ventricular-like hiPSC-CM. APs elicited at 1 Hz by a 3-ms stimulus of 100 pA. Note difference in time scale between panels **(A,B)**.

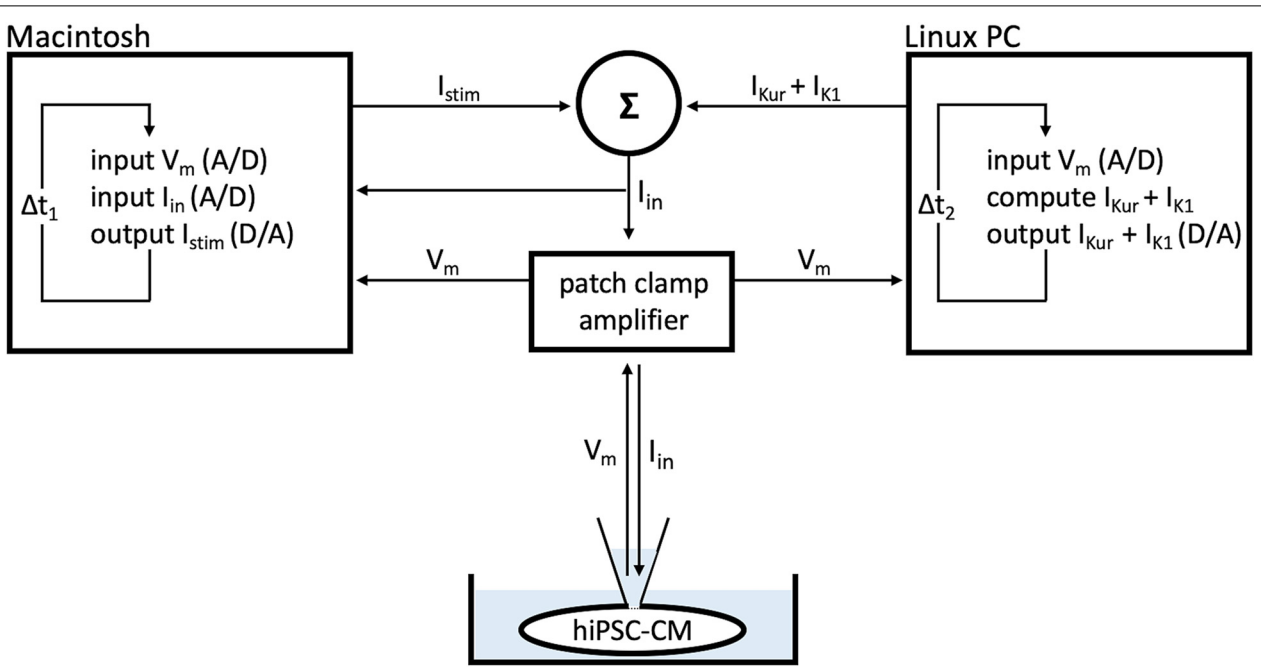

FIGURE 2 | Dynamic clamp setup. Ultrarapid delayed rectifier K^+ current (I_{Kur}) and inward rectifier potassium current (I_{K1}) were computed in real time on a PC running the Linux operating system and Real-Time Experiment Interface (RTXI) software (Patel et al., 2017), based on the acquired membrane potential (V_m) of the human induced pluripotent stem cell-derived cardiomyocyte (hiPSC-CM). Data were recorded on an Apple Macintosh computer using custom software to visualize and control the experiment. The sum of the stimulus current (I_{stim}), I_{K1}, and I_{Kur} resulted in the current that was injected into the hiPSC-CM (I_{in}). Sample rates were 30 kHz (Δt_1 = 33.33 μs) and 20 kHz (Δt_2 = 50 μs).

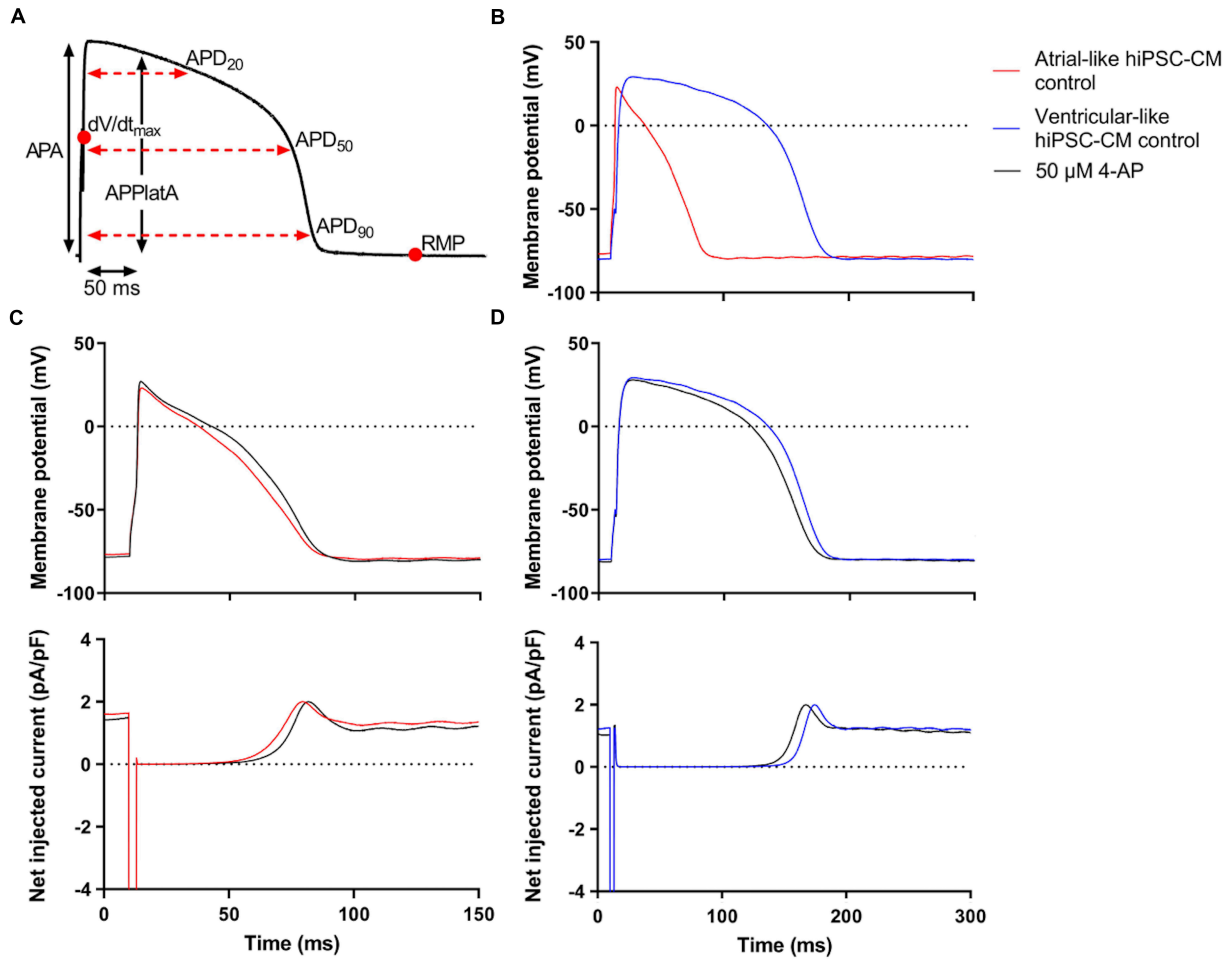

FIGURE 3 | Control atrial- and ventricular-like hiPSC-CM APs. **(A)** AP parameters used for analysis: resting membrane potential (RMP), maximum upstroke velocity (dV/dt_{max}), AP amplitude (APA), AP duration at 20, 50, and 90% repolarization (APD_{20}, APD_{50}, and APD_{90}, respectively), and AP plateau amplitude at 50 ms after reaching dV/dt_{max} (APPlatA). **(B)** Superimposed typical APs of an atrial-like hiPSC-CM (red line) and a ventricular-like hiPSC-CM (blue line). **(C)** Superimposed APs (top panel) and associated net current consisting of stimulus current and virtual I_{K1} injected through dynamic clamp (bottom panel) of an atrial-like hiPSC-CM in absence (red line) and presence of 50 µM 4-aminopyridine (4-AP) (black line). **(D)** Superimposed APs (top panel) and associated net injected current (bottom panel) of a ventricular-like hiPSC-CM. APs elicited at 1 Hz by a 3-ms stimulus of 100 pA. Note difference in time scale between panels **(C,D)**.

comparing AP parameters of atrial- and ventricular-like hiPSC-CMs in absence or presence of 4-AP. One-way repeated measures ANOVA followed by the Student–Newman–Keuls *post hoc* test was used for comparing the effect of injecting virtual I_{Kur} at various densities into atrial- and ventricular-like hiPSC-CMs. $P < 0.05$ was considered statistically significant.

RESULTS

Atrial- and Ventricular-Like hiPSC-CM APs

APs were recorded from single atrial- and ventricular-like hiPSC-CMs that showed spontaneous beating upon visual inspection, clearly indicating a healthy and myocardial status. APs were elicited at 1 Hz and virtual I_{K1} was injected into the cells, based on the approach of Meijer van Putten et al. (2015), to stabilize the RMP and set it at a regular hyperpolarized value. **Figure 3B** shows typical atrial- and ventricular-like hiPSC-CM APs. AP parameters, as illustrated in **Figure 3A**, are summarized in **Table 1**. Atrial-like hiPSC-CMs repolarize faster than ventricular-like APs, resulting in a significantly shorter APD_{20}, APD_{50}, and APD_{90}. The ventricular-like APs have a prominent plateau phase at relatively positive potentials, in contrast with the atrial-like hiPSC-CMs that show a less prominent plateau phase at less positive potentials, if any plateau at all. Consequently, APPlatA was significantly smaller in atrial-like hiPSC-CMs and thus appeared a strong tool to distinguish between atrial-like and ventricular-like hiPSC-CMs. APA and dV/dt_{max} did not differ between the atrial- and ventricular-like hiPSC-CMs, but RMP was less negative in ventricular-like hiPSC-CMs.

Next, the cells were superfused with 50 µM 4-AP to block intrinsic I_{Kur}. **Figures 3C,D**, top panels, show typical atrial- and ventricular-like hiPSC-CMs in absence (red and blue lines,

TABLE 1 | AP parameters of atrial- and ventricular-like hiPSC-CMs in absence and presence of 4-AP.

	Atrial-like hiPSC-CMs (n = 11)		Ventricular-like hiPSC-CMs (n = 10)	
	Baseline	**4-AP**	**Baseline**	**4-AP**
RMP (mV)	−81.31 ± 0.43	−80.83 ± 0.65	−75.52 ± 1.69*	−74.92 ± 1.71#
dV/dt_{max} (V/s)	74.54 ± 13.10	76.47 ± 13.41	83.70 ± 20.21	94.33 ± 24.43
APA (mV)	96.61 ± 2.66	98.33 ± 1.44	105.61 ± 3.69	104.59 ± 3.88
APD_{20} (ms)	35.86 ± 4.35	38.13 ± 4.69	77.73 ± 11.59*	68.68 ± 10.67‡#
APD_{50} (ms)	60.99 ± 5.55	65.05 ± 5.38	127.93 ± 19.67*	119.41 ± 18.09‡#
APD_{90} (ms)	81.27 ± 6.37	86.76 ± 5.92†	155.01 ± 21.49*	147.68 ± 20.38‡#
APPlatA (mV)	53.61 ± 5.25	60.53 ± 4.53†	89.61 ± 4.51*	89.42 ± 4.30#

*Data are AP parameters (mean ± SEM) of APs elicited at 1 Hz in absence (baseline) and presence of 50 μM 4-aminopyridine (4-AP). *P < 0.05 atrial- vs. ventricular-like hiPSC-CMs (baseline); †P < 0.05 4-AP vs. baseline of atrial-like hiPSC-CMs; ‡P < 0.05 4-AP vs. baseline of ventricular-like hiPSC-CMs; #P < 0.05 atrial- vs. ventricular-like hiPSC-CMs (4-AP).*

respectively) and presence of 4-AP (black lines). The associated injected currents, which each consist of I_{K1} and the 3-ms stimulus current applied at 10 ms, are displayed in the bottom panels of **Figures 3C,D**. In atrial-like hiPSC-CMs, I_{Kur} blockade resulted in a significantly increased APD_{90} and APPlatA, while other AP parameters were unaffected (**Table 1**). In contrast, in ventricular-like hiPSC-CMs, APD_{20}, APD_{50} and APD_{90} were significantly decreased upon I_{Kur} blockade (**Table 1**). The small AP shortening likely results from a time effect rather than a drug effect because I_{Kur} is virtually absent in our ventricular-like hiPSC-CMs. Comparing atrial- with ventricular-like APs during I_{Kur} blockade, most AP parameters still differ significantly, except APA and dV/dt_{max}.

Native I_{Kur}

Native I_{Kur} density in atrial- and ventricular-like hiPSC-CMs was quantified during 200-ms depolarizing voltage clamp steps as the current sensitive to 50 μM 4-AP. **Figure 4A** shows typical examples in an atrial-like (red trace) and a ventricular-like hiPSC-CM (blue trace). On average, I_{Kur} density in atrial-like hiPSC-CMs was significantly larger than in ventricular-like hiPSC-CMs, with densities of 1.88 ± 0.49 (n = 17) and 0.26 ± 0.26 (n = 17) pA/pF, respectively (**Figure 4B**).

If the voltage clamp protocol of **Figure 4A** is repeated in computer simulations with the Maleckar et al. (2009) human atrial myocyte model (Wilders, 2018), an I_{Kur} density of 5.45 pA/pF is obtained. We regard the latter as a realistic value for human atrial myocytes since Maleckar et al. (2009) based the characteristics of their model I_{Kur} on experimental data on I_{Kur} from isolated human atrial myocytes.

Effects of Baseline Virtual I_{Kur} on APs of Atrial- and Ventricular-Like hiPSC-CMs

Next, we studied the effects of a virtual I_{Kur} on APs of atrial and ventricular-like hiPSC-CMs using dynamic clamp. In the human heart, I_{Kur} is highly atrial-specific (Ellinghaus et al., 2005; Gaborit et al., 2007). However, the dynamic clamp technique allowed us to inject a virtual I_{Kur} in both atrial- and ventricular-like hiPSC-CMs and thus assess to which extent this made their action potential morphology become similar. In either case, 4-AP (50 μM) was present to ensure that any native I_{Kur} was blocked (Wang et al., 1993) and from here on we name this condition 0% I_{Kur}. First, we injected a virtual I_{Kur} as implemented in the Maleckar et al. (2009) human atrial myocyte model, i.e., with the aforementioned 5.45 pA/pF density at +50 mV, which we here consider as 100% density.

Figures 5A,B, top panels, show typical examples of APs recorded from atrial- and ventricular-like hiPSC-CM at 0% (red and blue lines, respectively) and 100% I_{Kur} (black lines). The injected current, which now consists of I_{K1}, 0% or 100% I_{Kur}, and a short stimulus current, is shown in the middle panels of **Figures 5A,B**. The average effects on the AP parameters of 11 atrial- and 10 ventricular-like hiPSC-CMs appear as the bars at 0% and 100% I_{Kur} in **Figures 6A–H**, **7A–F**, in which each of the AP parameters is expressed as a percentage of its value obtained at 100% I_{Kur}. Injection of I_{Kur} shortened the AP of both atrial- and ventricular-like hiPSC-CMs, while the AP plateau was suppressed (**Figures 5**, **6**). dV/dt_{max} was unaltered in both atrial- and ventricular-like hiPSC-CMs, but in atrial-like hiPSC-CMs RMP was significantly more negative and APA significantly larger in absence than in presence of I_{Kur} (**Figure 7**). The small 1.2% difference in RMP, equivalent to a 1.0-mV hyperpolarization, is likely a false positive because injection of various amounts of I_{Kur} did not affect the RMP in either atrial-like or ventricular-like hiPSC-CMs (see below).

The phase plane plots of **Figures 5C,D** show the injected currents of the middle panels of **Figures 5A,B** plotted against the associated membrane potentials of the APs shown in the top panels of **Figures 5A,B**. The start and the end of the negative depolarizing current that flows during the stimulus are indicated by downward and upward vertical arrows, respectively. The black loops of the phase plane plots clearly show that I_{Kur} is a repolarizing current that is already activated during the 3-ms stimulus and stays active until repolarization reaches −40 to −50 mV and the black traces 'fuse' with the red and blue traces of the action potentials without I_{Kur} (horizontal arrows). At these negative potentials, I_{Kur} becomes small because of both deactivation—rather than inactivation, which is much slower—and diminishing driving forces. The maximum I_{Kur} during the atrial-like AP is slightly larger compared to the ventricular-like AP because in this particular example the atrial-like AP reaches a higher peak than the ventricular-like AP, which results in a larger driving force for I_{Kur}.

Effects of I_{Kur} Loss-of-Function Mutations in Atrial- and Ventricular-Like hiPSC-CMs

Next, we studied the effects of loss-of-function mutations in *KCNA5*, resulting in a decrease in I_{Kur}. Therefore, we decreased the fully activated conductance of the virtual I_{Kur} conductance to 75, 50, 25, and 12.5% of its control value. **Figure 8** shows typical examples of the effects on the APs of atrial- and ventricular-like hiPSC-CMs. The average changes

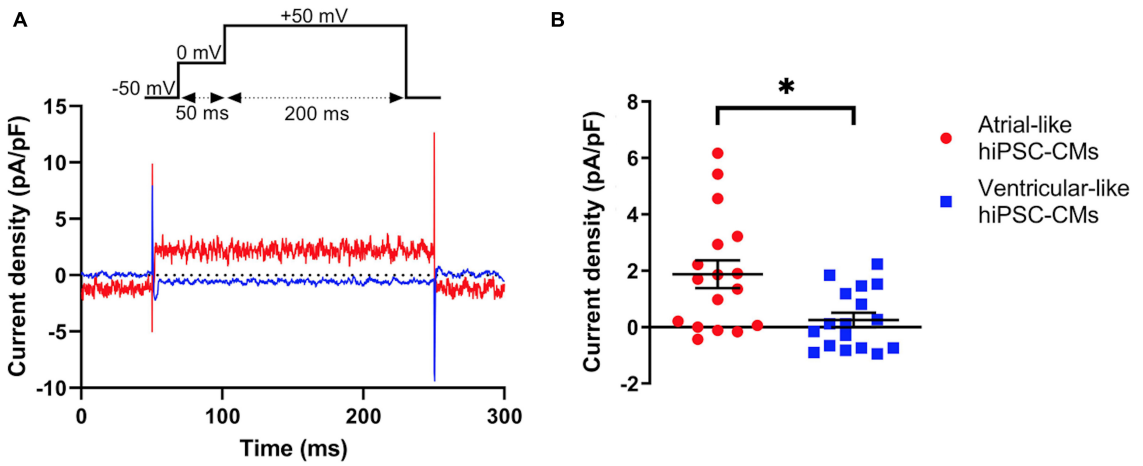

FIGURE 4 | Density of I_{Kur} measured as 50 μM 4-AP-sensitive current. **(A)** Typical 4-AP-sensitive currents in an atrial- and a ventricular-like hiPSC-CM (red and blue traces, respectively) upon 200-ms depolarizing voltage clamp steps to +50 mV from a holding potential of −50 mV. **(B)** I_{Kur} density in 17 atrial- and 17 ventricular-like hiPSC-CMs. *$P < 0.05$.

in AP parameters are shown in **Figures 6**, **7**. In both atrial- and ventricular-like hiPSC-CMs, APD_{20}, APD_{50}, and APD_{90} significantly increased upon a reduction in I_{Kur} (**Figures 6A–F**). However, while the increase in APD_{90} in atrial-like APs is only present upon severe I_{Kur} reduction, APD_{90} prolongation in ventricular-like APs is already present at a mild reduction (**Figures 6E,F**). APPlatA was significantly increased in both atrial- and ventricular-like APs (**Figures 6G,H**). RMP and dV/dt_{max} were unaffected (**Figures 7A–D**), whereas a slight increase in APA was observed, but only in atrial-like hiPSC-CMs at severe reductions of I_{Kur} (**Figures 7E,F**).

Effects of I_{Kur} Gain-of-Function Mutations in Atrial- and Ventricular-Like hiPSC-CMs

Finally, we studied the effects of gain-of-function mutations in *KCNA5*, resulting in an increase in I_{Kur}. Therefore, we increased the fully activated conductance of the virtual I_{Kur} conductance to 125, 150, 175, and 200% of its control value. **Figure 9** shows typical examples of the effects on the APs of atrial- and ventricular-like hiPSC-CMs. The average changes in AP parameters are shown in **Figures 6**, **7**. In both atrial- and ventricular-like hiPSC-CMs, APD_{20} and APD_{50} significantly shortened, but only when I_{Kur} was strongly increased (**Figures 6A–D**). APD_{90} was significantly reduced in ventricular-like, but not in atrial-like hiPSC-CMs (**Figures 6E,F**). APPlatA only showed a significant decrease in ventricular-like hiPSC-CMs (**Figures 6G,H**). Other AP parameters were unaffected upon increases in I_{Kur} (**Figure 7**).

DISCUSSION

Overall, the APs of our atrial-like hiPSC-CMs were substantially shorter and had a lower AP plateau than those of our ventricular-like hiPSC-CMs, in qualitative agreement with previous studies on atrial- and ventricular-like hiPSC-CMs (Marczenke et al., 2017; Verkerk et al., 2017; Argenziano et al., 2018; Cyganek et al., 2018; Lemme et al., 2018; Veerman et al., 2019). There are some quantitative differences in AP parameters with previous studies, but these are likely due to differences in cell lines, differences in differentiation protocols, absence or presence of I_{K1} injection, and a different definition of AP plateau amplitude. The differences in AP parameters of our atrial- and ventricular-like hiPSC-CMs would have been even larger if we had supplied our atrial-like hiPSC-CMs with a more atrial-specific I_{K1}, as not only observed in human heart (Wang et al., 1998), but also in canine, murine and sheep heart (Dhamoon et al., 2004; Panama et al., 2007; Cordeiro et al., 2015). Of note, Fabbri et al. (2019) recently published a detailed *in silico* study of the effects of several I_{K1} formulations on AP duration of hiPSC-CMs.

Maximum sustained native I_{Kur} density was larger in our atrial-like hiPSC-CMs than in our ventricular-like hiPSC-CMs. Yet, with a value of 1.88 ± 0.49 pA/pF at +50 mV, the I_{Kur} density of our atrial-like hiPSC-CMs was small in comparison with that of freshly isolated human atrial myocytes, for which Amos et al. (1996) observed a density of 5.1 ± 0.3 pA/pF for peak I_{Kur} and 4.7 ± 0.2 pA/pF for late I_{Kur} during a 300-ms voltage clamp step to +40 mV at 22°C (114 cells, 32 hearts). Therefore, we decided to block native I_{Kur} and use dynamic clamp to study the effects of I_{Kur}, using a virtual I_{Kur} with characteristics, including its density, based on observations made in freshly isolated human atrial myocytes.

Due to the relatively low native I_{Kur} density of our atrial- and ventricular-like hiPSC-CMs, it was not surprising that blockade of I_{Kur} by 4-AP had only minor effects on AP parameters. When native I_{Kur} was replaced with virtual I_{Kur} with 100% density, similar to I_{Kur} density in freshly isolated human atrial myocytes, more pronounced effects on AP parameters were observed. In atrial-like hiPSC-CMs, APD_{20} shortened substantially, whereas APD_{50} shortened only moderately and APD_{90} even less so. In ventricular-like hiPSC-CMs, on the other hand, not only

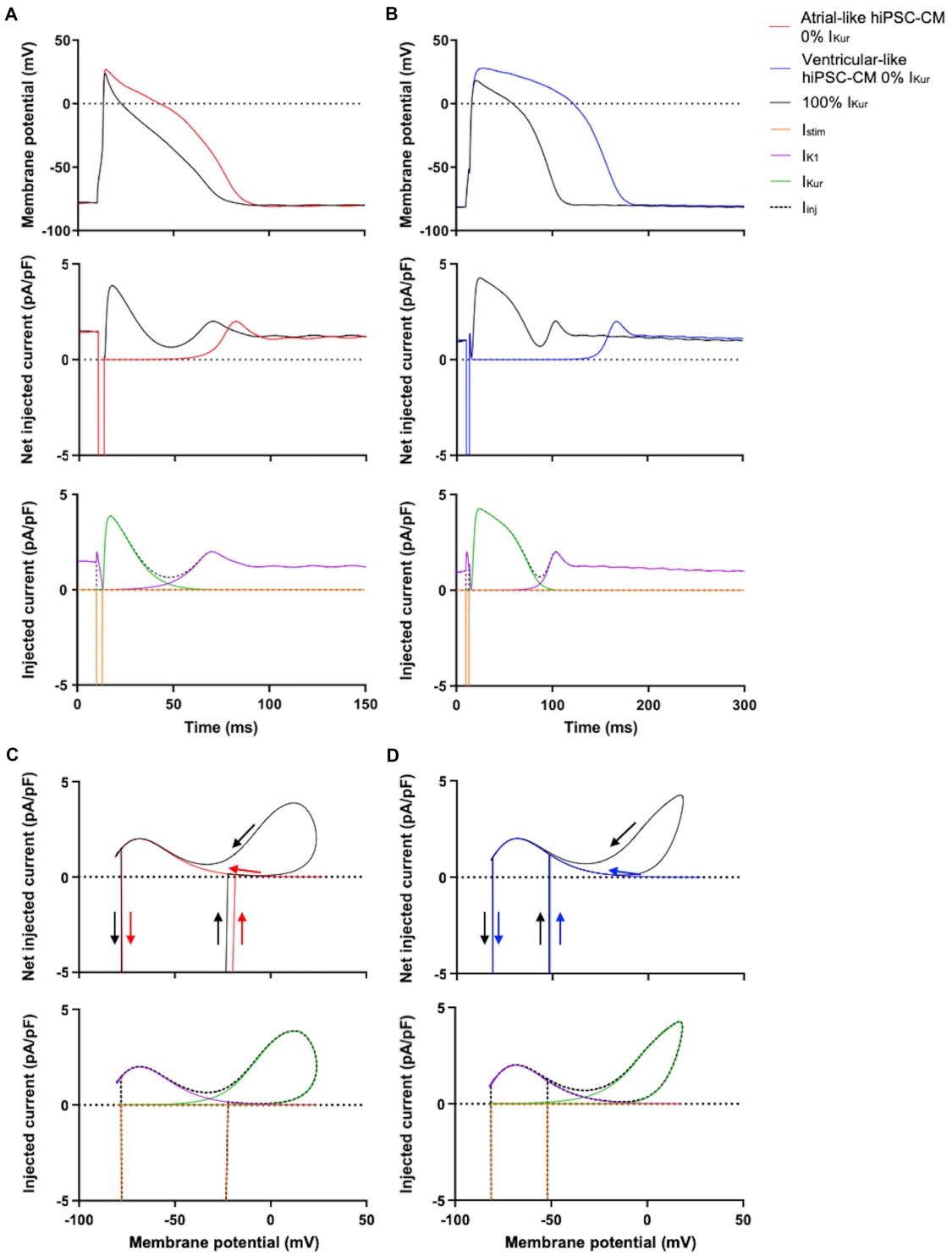

FIGURE 5 | Effect of injection of 100% virtual I_{Kur} through dynamic clamp on APs of atrial- and ventricular-like hiPSC-CMs. **(A)** Superimposed APs (top panel) of an atrial-like hiPSC-CM at 0% (red line) and 100% virtual I_{Kur} (black line) and associated net injected current (middle panel), consisting of I_{K1}, 0% or 100% I_{Kur}, and a short stimulus current, as shown in the bottom panel in case of 100% I_{Kur}. **(B)** Superimposed APs (top panel), associated net injected current (middle panel), and its individual components in case of 100% I_{Kur} (bottom panel) of a ventricular-like hiPSC-CM. **(C,D)** Phase plane plots (top panel) of the action potentials and injected currents of panels **(A,B)** with their individual components in case of 100% I_{Kur} (bottom panel). APs elicited at 1 Hz by a 3-ms stimulus of 100 pA. Note difference in time scale between panels **(A,B)**.

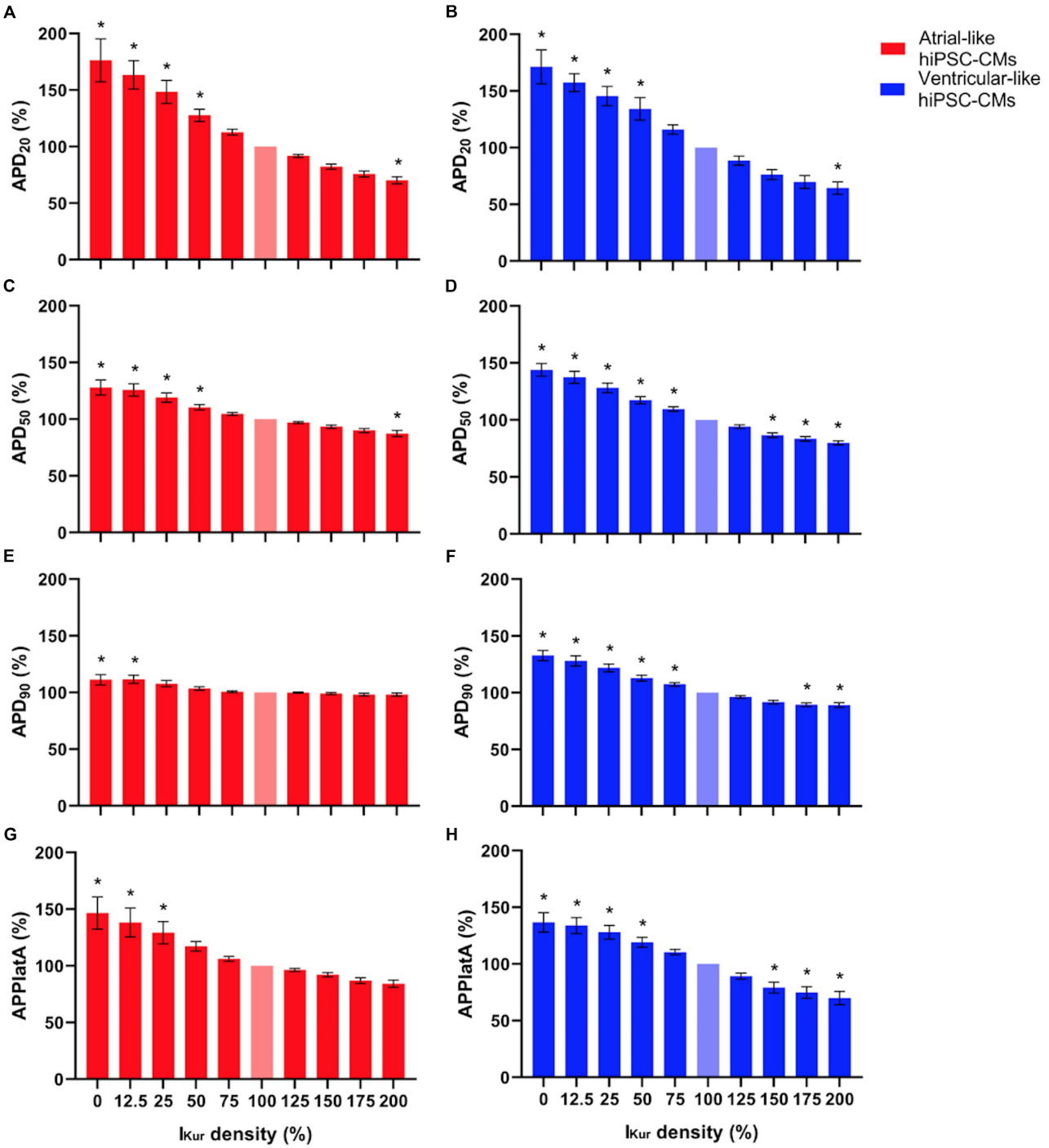

FIGURE 6 | (A,B) APD_{20}, **(C,D)** APD_{50}, **(E,F)** APD_{90}, and **(G,H)** APPlatA of atrial- and ventricular-like hiPSC-CMs (left and right panels, respectively) at virtual I_{Kur} densities ranging from 0 to 200%. AP parameters are expressed as percentage relative to their value at 100% I_{Kur} density (bleached bars). Data from 11 atrial- and 10 ventricular-like hiPSC-CMs. *$P < 0.05$.

APD_{20}, but also APD_{50} and APD_{90} shortened substantially upon injection of virtual I_{Kur}. The more pronounced effect on APD in ventricular-like hiPSC-CMs is likely related to the longer and more positive AP plateau potentials leading to more functional consequences of I_{Kur}. The observed decrease in APD_{20} was accompanied by a lowering of the AP plateau in both atrial- and ventricular-like hiPSC-CMs.

We only performed experiments at a pacing rate of 1 Hz and not at higher pacing rates. Therefore, we were unable to confirm that the relative contribution of I_{Kur} to AP repolarization

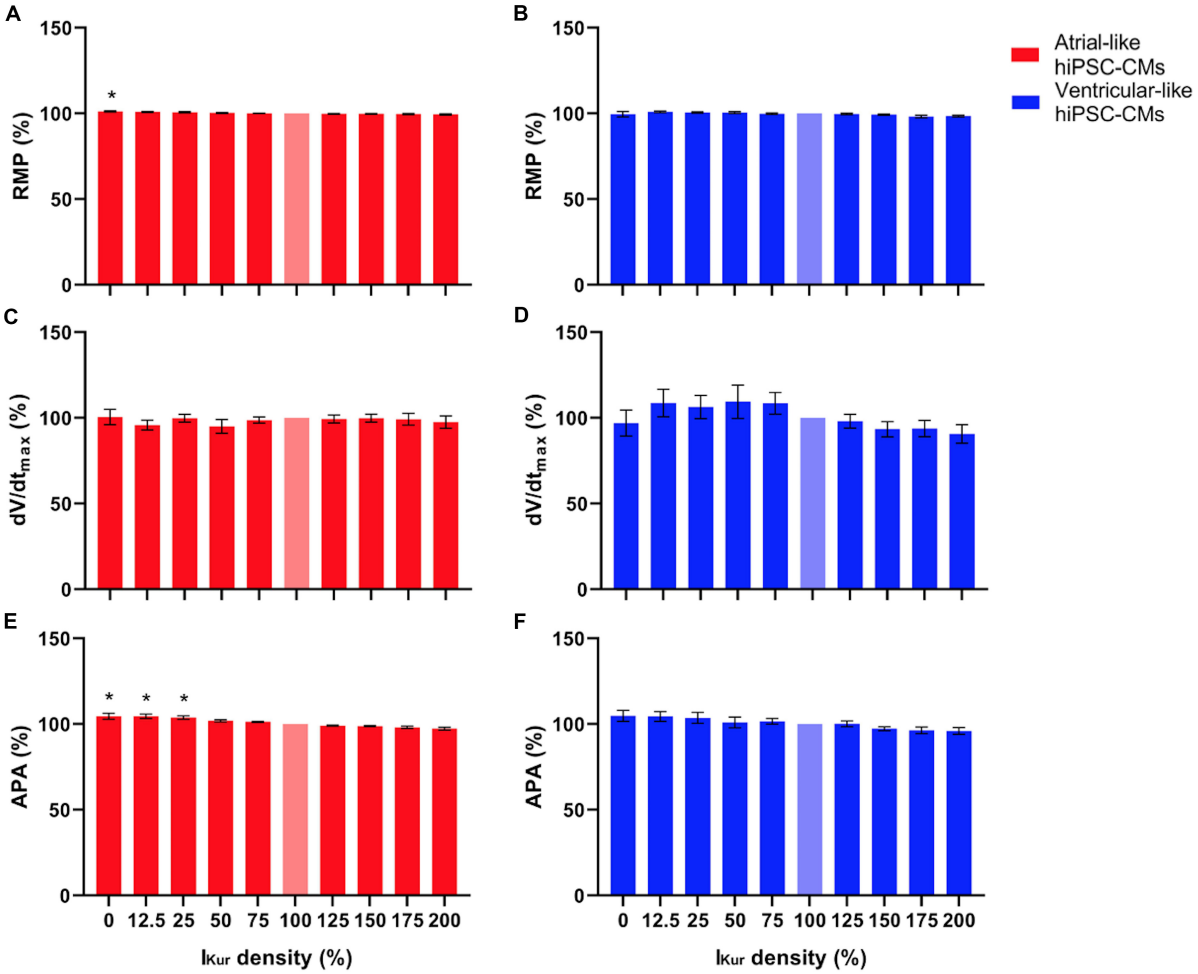

FIGURE 7 | (A,B) RMP, **(C,D)** dV/dt_{max}, and **(E,F)** APA of atrial- and ventricular-like hiPSC-CMs (left and right panels, respectively) at virtual I_{Kur} densities ranging from 0 to 200%. AP parameters are expressed as percentage relative to their value at 100% I_{Kur} density (bleached bars). Data from 11 atrial- and 10 ventricular-like hiPSC-CMs. $^*P < 0.05$.

increases with increasing pacing rate (Ford et al., 2016; Aguilar et al., 2017). Aguilar et al. (2017) carried out comprehensive computer simulations with the Courtemanche et al. (1998) human atrial myocyte model, in which the I_{Kur} formulation was updated in accordance with the experimental observations on I_{Kur} inactivation by Feng et al. (1998). They found that I_{Kur} did not inactivate significantly at high pacing rates and, consequently, the contribution of I_{Kur} to repolarization was mainly determined by its (fast) activation kinetics. Accordingly, rate-dependent changes in I_{Kur} were largely determined by changes in action potential morphology. In computer simulations with the Maleckar et al. (2009) model, on which we based our I_{Kur} formulation, we made similar observations (data not shown). We aim to test the rate dependence of the effects of I_{Kur} on AP repolarization in future experiments on hiPSC-CMs.

In both atrial- and ventricular-like hiPSC-CMs, simulation of loss-of-function mutations through lowering of the virtual I_{Kur} density from 100% to 12.5–75% of its control value, resulted in prolongation of the AP and raise of its plateau, in line with the differences in AP parameters that were observed between 0 and 100% I_{Kur}. Marczenke et al. (2017) found that knock-out of *KCNA5* in hiPSC-CMs, representing a complete loss-of-function, may result in the development of EADs, which, however, were not observed in the present study, likely due to our higher pacing frequency. At I_{Kur} densities > 100%, simulating gain-of-function mutations, effects on AP parameters were somewhat less pronounced. In both atrial- and ventricular-like hiPSC-CMs, APD_{20} was only significantly decreased upon an increase in I_{Kur} density to 200%. A significant lowering of the AP plateau, together with AP shortening, was only observed in ventricular-like hiPSC-CMs.

Although the sustained native I_{Kur} density at +50 mV was small in our atrial-like hiPSC-CMs (1.88 ± 0.49 pA/pF, $n = 17$), it was still significantly larger than in our ventricular-like hiPSC-CMs (0.26 ± 0.26 pA/pF, $n = 17$). Within our atrial-like hiPSC-CM population we noted cells lacking I_{Kur} (**Figure 4B**), although atrial-like hiPSC-CM generation using retinoic acid has been shown to generate 90–95% atrial-like hiPSC-CMs

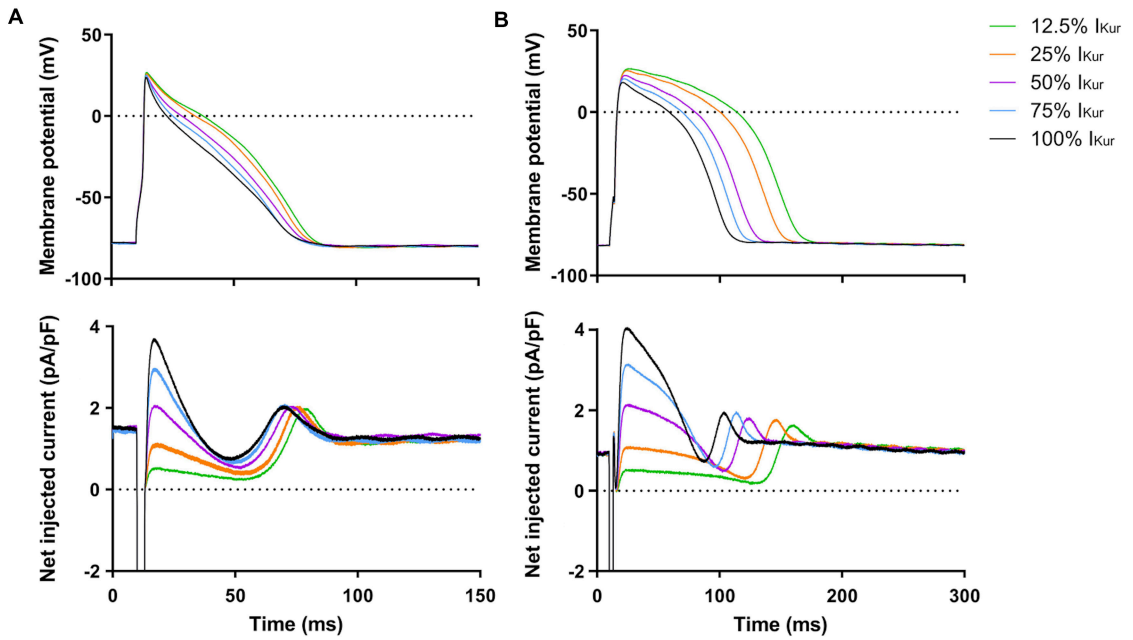

FIGURE 8 | Effect of I_{Kur} loss-of-function mutations on APs of atrial- and ventricular-like hiPSC-CMs. **(A)** Superimposed APs of an atrial-like hiPSC-CM upon injection of 12.5–100% virtual I_{Kur} through dynamic clamp and associated injected current (bottom panel), consisting of I_{K1}, 12.5–100% I_{Kur}, and a short stimulus current. **(B)** Superimposed APs (top panel) and associated injected current (bottom panel) of a ventricular-like hiPSC-CM. APs elicited at 1 Hz by a 3-ms stimulus of 100 pA. Note difference in time scale between panels **(A,B)**.

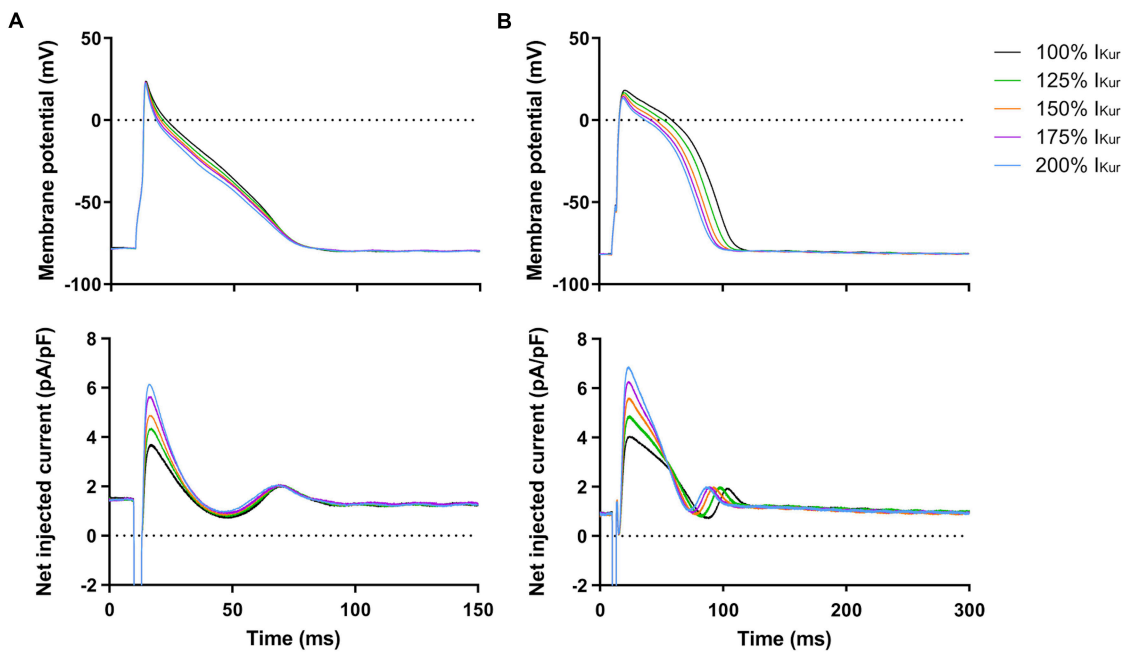

FIGURE 9 | Effect of I_{Kur} gain-of-function mutations on APs of atrial- and ventricular-like hiPSC-CMs. **(A)** Superimposed APs of an atrial-like hiPSC-CM upon injection of 100–200% virtual I_{Kur} through dynamic clamp and associated injected current (bottom panel), consisting of I_{K1}, 100–200% I_{Kur}, and a short stimulus current. **(B)** Superimposed APs (top panel) and associated injected current (bottom panel) of a ventricular-like hiPSC-CM. APs elicited at 1 Hz by a 3-ms stimulus of 100 pA. Note difference in time scale between panels **(A,B)**.

(Cyganek et al., 2018), with the rest being sinus- or ventricular-like hiPSC-CMs. Since hiPSC-CMs display an immature phenotype, it is possible that not all atrial-like hiPSC-CMs have developed I_{Kur} densities large enough to be detected as 4-AP sensitive current in a voltage clamp setting. Our recorded I_{Kur} densities are lower than those of the only other known quantification of I_{Kur} density in atrial- and ventricular-like hiPSC-CMs (Kaplan et al., 2016). In the study by Kaplan et al. (2016), which has only been published in abstract form, the sustained I_{Kur} density at +50 mV amounted to 3.71 ± 0.55 pA/pF (n = 5) in atrial-like hiPSC-CMs, which was significantly larger than that of ventricular-like hiPSC-CMs (1.00 ± 0.10 pA/pF, n = 16). To distinguish between the two types of hiPSC-CMs based on I_{Kur} densities would require further investigation, although the available data suggest a trend of a significantly larger I_{Kur} density in atrial-like hiPSC-CMs.

Of note, all AP parameters of our atrial- and ventricular-like hiPSC-CMs except dV/dt_{max} and APA were not only different under control conditions, but also upon blockade of I_{Kur} by 4-AP, indicating that the two types of hiPSC-CMs are not only different in their level of $K_v1.5$ expression, as determined by I_{Kur} density, and suggesting that differences in membrane currents other than I_{Kur} also contribute to the observed differences in AP parameters. This result is in line with previous findings by both Marczenke et al. (2017) and Lemme et al. (2018), who found that knock-out of *KCNA5* or I_{Kur} blockade by 4-AP in atrial-like hiPSC-CMs did not result in completely ventricular-like APs. These findings are, however, to some extent at odds with those by Kaplan et al. (2016), who noticed that the APs of their atrial-like hiPSC-CMs took on a ventricular-like shape when treated with 4-AP, which strongly suggested that I_{Kur} is the major determinant of atrial action potential morphology. Conversely, they observed that injection of a virtual I_{Kur} in ventricular-like hiPSC-CMs, employing the dynamic clamp technique using oocytes expressing a cloned $K_v1.5$ current, resulted in APs similar to those of atrial-like hiPSC-CMs. Apart from the studies by Kaplan et al. (2016), Marczenke et al. (2017), and Lemme et al. (2018), data on I_{Kur} in hiPSC-CMs are limited and the electrophysiology of I_{Kur} in atrial- and ventricular-like hiPSC-CMs remains largely unknown.

Apart from demonstrating a link between altered I_{Kur} density and changes in AP parameters, I_{Kur} has now been quantified in both atrial- and ventricular-like hiPSC-CMs. Thus, the present study provides additional data toward a complete characterization of individual membrane currents in hiPSC-CMs. Moreover, our study illustrates the potentials of dynamic clamp experiments on hiPSC-CMs, allowing manipulation of characteristics of the injected current in real time, thus facilitating direct, systematic, and efficient testing of changes in those characteristics. In the context of studying drug effects, including effects of anti-AF drugs, dynamic clamp may prove useful in the identification of potential drug targets and in testing model-based hypotheses (Ortega et al., 2018). For instance, dynamic clamp experiments on atrial-like hiPSC-CMs with I_{Kur} based on specific loss- or gain-of-function mutations in *KCNA5* can be utilized to assess the cellular effects of these mutations as well as effects of dedicated pharmacological treatment through modulation of I_{Kur}. Ultimately, this may lead to mutation-specific treatment of AF.

DATA AVAILABILITY STATEMENT

The raw data supporting the conclusions of this article will be made available by the authors, without undue reservation.

AUTHOR CONTRIBUTIONS

SH designed and performed the experiments, analyzed the data, and drafted the manuscript. HD cultured the hiPSC line and developed the procedures to generate atrial-like and ventricular-like hiPSC-CMs. LB prepared the hiPSC-CMs used for electrophysiology in the present study. AV and RW designed the study, interpreted the data, and drafted, edited, and approved the manuscript.

FUNDING

Dr. Harsha D. Devalla is supported by a ZonMW and Hartstichting MKMD grant (114021512).

REFERENCES

Aguilar, M., Feng, J., Vigmond, E., Comtois, P., and Nattel, S. (2017). Rate-dependent role of I_{Kur} in human atrial repolarization and atrial fibrillation maintenance. *Biophys. J.* 112, 1997–2010. doi: 10.1016/j.bpj.2017.03.022

Amos, G. J., Wettwer, E., Metzger, F., Li, Q., Himmel, H. M., and Ravens, U. (1996). Differences between outward currents of human atrial and subepicardial ventricular myocytes. *J. Physiol.* 491, 31–50. doi: 10.1113/jphysiol.1996.sp021194

Argenziano, M., Lambers, E., Hong, L., Sridhar, A., Zhang, M., Chalazan, B., et al. (2018). Electrophysiologic characterization of calcium handling in human induced pluripotent stem cell-derived atrial cardiomyocytes. *Stem Cell Rep.* 10, 1867–1878. doi: 10.1016/j.stemcr.2018.04.005

Barry, P. H., and Lynch, J. W. (1991). Liquid junction potentials and small cell effects in patch-clamp analysis. *J. Membr. Biol.* 121, 101–117. doi: 10.1007/BF01870526

Caballero, R., De la Fuente, M. G., Gómez, R., Barana, A., Amorós, I., Dolz-Gaitón, P., et al. (2010). In humans, chronic atrial fibrillation decreases the transient outward current and ultrarapid component of the delayed rectifier current differentially on each atria and increases the slow component of the delayed rectifier current in both. *J. Am. Coll. Cardiol.* 55, 2346–2354. doi: 10.1016/j.jacc.2010.02.028

Christophersen, I. E., Olesen, M. O., Liang, B., Andersen, M. A., Larsen, A. P., Nielsen, J. B., et al. (2013). Genetic variation in *KCNA5*: impact on the atrial-specific potassium rectifier current I_{Kur} in patients with lone atrial fibrillation. *Eur. Heart J.* 34, 1517–1525. doi: 10.1093/eurheartj/ehs442

Colman, M. A., Ni, H., Liang, B., Schmidt, N., and Zhang, H. (2017). *In silico* assessment of genetic variation of *KCNA5* reveals multiple mechanisms of human atrial arrhythmogenesis. *PLoS Comput. Biol.* 13:e1005587. doi: 10.1371/journal.pcbi.1005587

Cordeiro, J. M., Zeina, T., Goodrow, R., Kaplan, A. D., Thomas, L. M., Nesterenko, V. V., et al. (2015). Regional variation of the inwardly rectifying potassium current in the canine heart and the contributions to differences in action potential repolarization. *J. Mol. Cell. Cardiol.* 84, 52–60. doi: 10.1016/j.yjmcc.2015.04.010

Courtemanche, M., Ramirez, R. J., and Nattel, S. (1998). Ionic mechanisms underlying human atrial action potential properties: insights from a mathematical model. *Am. J. Physiol.* 275, H301–H321. doi: 10.1152/ajpheart.1998.275.1.H301

Cyganek, L., Tiburcy, M., Sekeres, K., Gerstenberg, K., Bohnenberger, H., Lenz, C., et al. (2018). Deep phenotyping of human induced pluripotent stem cell–derived atrial and ventricular cardiomyocytes. *JCI Insight* 3:e99941. doi: 10.1172/jci.insight.99941

Darbar, D., Herron, K. J., Ballew, J. D., Jahangir, A., Gersh, B. J., Shen, W. K., et al. (2003). Familial atrial fibrillation is a genetically heterogeneous disorder. *J. Am. Coll. Cardiol.* 41, 2185–2192. doi: 10.1016/S0735-1097(03)00465-0

Devalla, H. D., Gélinas, R., Aburawi, E. H., Beqqali, A., Goyette, P., Freund, C., et al. (2016). *TECRL*, a new life-threatening inherited arrhythmia gene associated with overlapping clinical features of both LQTS and CPVT. *EMBO Mol. Med.* 8, 1390–1408. doi: 10.15252/emmm.201505719

Devalla, H. D., and Passier, R. (2018). Cardiac differentiation of pluripotent stem cells and implications for modeling the heart in health and disease. *Sci. Transl. Med.* 10:eaah5457. doi: 10.1126/scitranslmed.aah5457

Devalla, H. D., Schwach, V., Ford, J. W., Milnes, J. T., El-Haou, S., Jackson, C., et al. (2015). Atrial-like cardiomyocytes from human pluripotent stem cells are a robust preclinical model for assessing atrial-selective pharmacology. *EMBO Mol. Med.* 7, 394–410. doi: 10.15252/emmm.201404757

Dhamoon, A. S., and Jalife, J. (2005). The inward rectifier current (I_{K1}) controls cardiac excitability and is involved in arrhythmogenesis. *Heart Rhythm* 2, 316–324. doi: 10.1016/j.hrthm.2004.11.012

Dhamoon, A. S., Pandit, S. V., Sarmast, F., Parisian, K. R., Guha, P., Li, Y., et al. (2004). Unique Kir2.x properties determine regional and species differences in the cardiac inward rectifier K^+ current. *Circ. Res.* 94, 1332–1339. doi: 10.1161/01.RES.0000128408.66946.67

Ellinghaus, P., Scheubel, R. J., Dobrev, D., Ravens, U., Holtz, J., Huetter, J., et al. (2005). Comparing the global mRNA expression profile of human atrial and ventricular myocardium with high-density oligonucleotide arrays. *J. Thoracic Cardiovasc. Surg.* 129, 1383–1390. doi: 10.1016/j.jtcvs.2004.08.031

Fabbri, A., Goversen, B., Vos, M. A., van Veen, T. A. B., and de Boer, T. P. (2019). Required G_{K1} to suppress automaticity of iPSC-CMs depends strongly on I_{K1} model structure. *Biophys. J.* 117, 2303–2315. doi: 10.1016/j.bpj.2019.08.040

Fedida, D., Wible, B., Wang, Z., Fermini, B., Faust, F., Nattel, S., et al. (1993). Identity of a novel delayed rectifier current from human heart with a cloned K^+ channel current. *Circ. Res.* 73, 210–216. doi: 10.1161/01.RES.73.1.210

Feghaly, J., Zakka, P., London, B., MacRae, C. A., and Refaat, M. M. (2018). Genetics of atrial fibrillation. *J. Am. Heart Assoc.* 7:e009884. doi: 10.1161/JAHA.118.009884

Feng, J., Xu, D., Wang, Z., and Nattel, S. (1998). Ultrarapid delayed rectifier current inactivation in human atrial myocytes: properties and consequences. *Am. J. Physiol.* 275, H1717–H1725. doi: 10.1152/ajpheart.1998.275.5.H1717

Ford, J., Milnes, J., El Haou, S., Wettwer, E., Loose, S., Matschke, K., et al. (2016). The positive frequency-dependent electrophysiological effects of the I_{Kur} inhibitor XEN-D0103 are desirable for the treatment of atrial fibrillation. *Heart Rhythm* 13, 555–564. doi: 10.1016/j.hrthm.2015.10.003

Gaborit, N., Le Bouter, S., Szuts, V., Varro, A., Escande, D., Nattel, S., et al. (2007). Regional and tissue specific transcript signatures of ion channel genes in the non-diseased human heart. *J. Physiol.* 582, 675–693. doi: 10.1113/jphysiol.2006.126714

Grandi, E., Pandit, S. V., Voigt, N., Workman, A. J., Dobrev, D., Jalife, J., et al. (2011). Human atrial action potential and Ca^{2+} model: sinus rhythm and chronic atrial fibrillation. *Circ. Res.* 109, 1055–1066. doi: 10.1161/CIRCRESAHA.111.253955

Hayashi, K., Konno, T., Tada, H., Tani, S., Liu, L., Fujino, N., et al. (2015). Functional characterization of rare variants implicated in susceptibility to lone atrial fibrillation. *Circulation* 8, 1095–1104. doi: 10.1161/CIRCEP.114.002519

Hoekstra, M., Mummery, C. L., Wilde, A. A. M., Bezzina, C. R., and Verkerk, A. O. (2012). Induced pluripotent stem cell derived cardiomyocytes as models for cardiac arrhythmias. *Front. Physiol.* 3:346. doi: 10.3389/fphys.2012.00346

Horváth, A., Lemoine, M. D., Löser, A., Mannhardt, I., Flenner, F., Uzun, A. U., et al. (2018). Low resting membrane potential and low inward rectifier potassium currents are not inherent features of hiPSC-derived cardiomyocytes. *Stem Cell Rep.* 10, 822–833. doi: 10.1016/j.stemcr.2018.01.012

hPSCreg (2019). *LUMCi004-A*. Available online at: https://hpscreg.eu/cell-line/LUMCi004-A (accessed March 31, 2020).

Kääb, S., Dixon, J., Duc, J., Ashen, D., Näbauer, M., Beuckelmann, D. J., et al. (1998). Molecular basis of transient outward potassium current downregulation in human heart failure: a decrease in Kv4.3 mRNA correlates with a reduction in current density. *Circulation* 98, 1383–1393. doi: 10.1161/01.CIR.98.14.1383

Kaplan, A. D., Rasmusson, R. L., and Bett, G. C. L. (2016). Ionic basis of repolarization of atrial and ventricular specific cell types derived from human induced pluripotent stem cells. *Biophys. J.* 110(Suppl. 1), 343a. doi: 10.1016/j.bpj.2015.11.1848

Lemme, M., Ulmer, B. M., Lemoine, M. D., Zech, A. T. L., Flenner, F., Ravens, U., et al. (2018). Atrial-like engineered heart tissue: an *in vitro* model of the human atrium. *Stem Cell Rep.* 11, 1378–1390. doi: 10.1016/j.stemcr.2018.10.008

Li, G.-R., Wang, H.-B., Qin, G.-W., Jin, M.-W., Tang, Q., Sun, H.-Y., et al. (2008). Acacetin, a natural flavone, selectively inhibits human atrial repolarization potassium currents and prevents atrial fibrillation in dogs. *Circulation* 117, 2449–2457. doi: 10.1161/CIRCULATIONAHA.108.769554

Maleckar, M. M., Greenstein, J. L., Giles, W. R., and Trayanova, N. A. (2009). K^+ current changes account for the rate dependence of the action potential in the human atrial myocyte. *Am. J. Physiol. Heart Circ. Physiol.* 297, H1398–H1410. doi: 10.1152/ajpheart.00411.2009

Marczenke, M., Piccini, I., Mengarelli, I., Fell, J., Röpke, A., Seebohm, G., et al. (2017). Cardiac subtype-specific modeling of $K_v1.5$ ion channel deficiency using human pluripotent stem cells. *Front. Physiol.* 8:469. doi: 10.3389/fphys.2017.00469

Mays, D. J., Foose, J. M., Philipson, L. H., and Tamkun, M. M. (1995). Localization of the Kv1.5 K^+ channel protein in explanted cardiac tissue. *J. Clin. Investig.* 96, 282–292. doi: 10.1172/JCI118032

Meijer van Putten, R. M. E., Mengarelli, I., Guan, K., Zegers, J. G., Van Ginneken, A. C. G., Verkerk, A. O., et al. (2015). Ion channelopathies in human induced pluripotent stem cell derived cardiomyocytes: a dynamic clamp study with virtual I_{K1}. *Front. Physiol.* 6:7. doi: 10.3389/fphys.2015.00007

Nattel, S. (2002). New ideas about atrial fibrillation 50 years on. *Nature* 415, 219–226. doi: 10.1038/415219a

Ng, E. S., Davis, R., Stanley, E. G., and Elefanty, A. G. (2008). A protocol describing the use of a recombinant protein-based, animal product-free medium (APEL) for human embryonic stem cell differentiation as spin embryoid bodies. *Nat. Protoc.* 3, 768–776. doi: 10.1038/nprot.2008.42

Ni, H., Adeniran, I., and Zhang, H. (2017). *In-silico* investigations of the functional impact of *KCNA5* mutations on atrial mechanical dynamics. *J. Mol. Cell. Cardiol.* 111, 86–95. doi: 10.1016/j.yjmcc.2017.08.005

Olson, T. M., Alekseev, A. E., Liu, X. K., Park, S., Zingman, L. V., Bienengraeber, M., et al. (2006). $K_v1.5$ channelopathy due to *KCNA5* loss-of-function mutation causes human atrial fibrillation. *Hum. Mol. Genet.* 15, 2185–2191. doi: 10.1093/hmg/ddl143

Ortega, F. A., Grandi, E., Krogh-Madsen, T., and Christini, D. J. (2018). Applications of dynamic clamp to cardiac arrhythmia research: role in drug target discovery and safety pharmacology testing. *Front. Physiol.* 8:1099. doi: 10.3389/fphys.2017.01099

Panama, B. K., McLerie, M., and Lopatin, A. N. (2007). Heterogeneity of I_{K1} in the mouse heart. *Am. J. Physiol. Heart Circ. Physiol.* 293, H3558–H3567. doi: 10.1152/ajpheart.00419.2007

Patel, Y. A., George, A., Dorval, A. D., White, J. A., Christini, D. J., and Butera, R. J. (2017). Hard real-time closed-loop electrophysiology with the Real-Time eXperiment Interface (RTXI). *PLoS Comput. Biol.* 13:e1005430. doi: 10.1371/journal.pcbi.1005430

Potpara, T. S., and Lip, G. Y. H. (2011). Lone atrial fibrillation: what is known and what is to come. *Int. J. Clin. Pract.* 65, 446–457. doi: 10.1111/j.1742-1241.2010.02618.x

Seltmann, S., Lekschas, F., Müller, R., Stachelscheid, H., Bittner, M.-S., Zhang, W., et al. (2016). hPSCreg—the human pluripotent stem cell registry. *Nucleic Acids Res.* 44, D757–D763. doi: 10.1093/nar/gkv963

Tian, L., Liu, G., Wang, L., Zheng, M., and Li, Y. (2015). KCNA5 gene polymorphism associate with idiopathic atrial fibrillation. *Int. J. Clin. Exp. Med.* 8, 9890–9896.

Veerman, C. C., Mengarelli, I., Koopman, C. D., Wilders, R., Van Amersfoorth, S. C., Bakker, D., et al. (2019). Genetic variation in *GNB5* causes bradycardia by augmenting the cholinergic response via increased acetylcholine-activated potassium current ($I_{K,ACh}$). *Dis. Models Mech.* 12:dmm037994. doi: 10.1242/dmm.037994

Verkerk, A. O., Veerman, C. C., Zegers, J. G., Mengarelli, I., Bezzina, C. R., and Wilders, R. (2017). Patch-clamp recording from human induced pluripotent stem cell-derived cardiomyocytes: improving action potential characteristics through dynamic clamp. *Int. J. Mol. Sci.* 18:1873. doi: 10.3390/ijms18091873

Wang, Z., Fermini, B., and Nattel, S. (1993). Sustained depolarization-induced outward current in human atrial myocytes: evidence for a novel delayed rectifier K^+ current similar to $K_v1.5$ cloned channel currents. *Circ. Res.* 73, 1061–1076. doi: 10.1161/01.RES.73.6.1061

Wang, Z., Yue, L., White, M., Pelletier, G., and Nattel, S. (1998). Differential distribution of inward rectifier potassium channel transcripts in human atrium versus ventricle. *Circulation* 98, 2422–2428. doi: 10.1161/01.cir.98.22.2422

Wettwer, E., Hála, O., Christ, T., Heubach, J. F., Dobrev, D., Knaut, M., et al. (2004). Role of I_{Kur} in controlling action potential shape and contractility in the human atrium: influence of chronic atrial fibrillation. *Circulation* 110, 2299–2306. doi: 10.1161/01.CIR.0000145155.60288.71

Wilders, R. (2006). Dynamic clamp: a powerful tool in cardiac electrophysiology. *J. Physiol.* 576, 349–359. doi: 10.1113/jphysiol.2006.115840

Wilders, R. (2018). Cellular mechanisms of sinus node dysfunction in carriers of the *SCN5A*-E161K mutation and role of the H558R polymorphism. *Front. Physiol.* 9:1795. doi: 10.3389/fphys.2018.01795

Yang, T., Yang, P., Roden, D. M., and Darbar, D. (2010). Novel KCNA5 mutation implicates tyrosine kinase signaling in human atrial fibrillation. *Heart Rhythm* 7, 1246–1252. doi: 10.1016/j.hrthm.2010.05.032

Yang, Y., Li, J., Lin, X., Yang, Y., Hong, K., Wang, L., et al. (2009). Novel KCNA5 loss-of-function mutations responsible for atrial fibrillation. *J. Hum. Genet.* 54, 277–283. doi: 10.1038/jhg.2009.26

Zhang, Q., Jiang, J., Han, P., Yuan, Q., Zhang, J., Zhang, X., et al. (2011). Direct differentiation of atrial and ventricular myocytes from human embryonic stem cells by alternating retinoid signals. *Cell Res.* 21, 579–587. doi: 10.1038/cr.2010.163

Conflict of Interest: The authors declare that the research was conducted in the absence of any commercial or financial relationships that could be construed as a potential conflict of interest.